Electronic Supplementary Material (ESI) for Soft Matter.

Supplementary Information for: Interactions and design rules for assembly of porous colloidal mesophases

Beth A. Lindquist, Sayantan Dutta, Ryan B. Jadrich, Delia J. Milliron, and Thomas M. Truskett*

McKetta Department of Chemical Engineering, University of Texas at Austin, Austin, TX 78712

E-mail: truskett@che.utexas.edu

Additional Characterization

In this Section, we provide additional details about the Iterative Boltzmann Inversion calculations, pore size distributions (PSDs), anisotropy factors, and characterization of potentials for a pore diameter of 5σ.

Comparison of Target and Optimized Radial Distribution Functions

In all cases, the matching between the radial distribution function of the target simulation and that of the optimized potential is excellent. Comparisons are shown in Fig. S1 for the packing fraction of the small particles in the IBI optimization, η_{opt}, of 0.31 at all prescribed pore diameters (d_{pore}) examined in this work, but the results of all other optimizations are comparable in quality. As in our prior work, the effect of the pores on $g(r)$ is relatively subtle, primarily manifest as a slight dip in the $g(r)$ around the pore size.

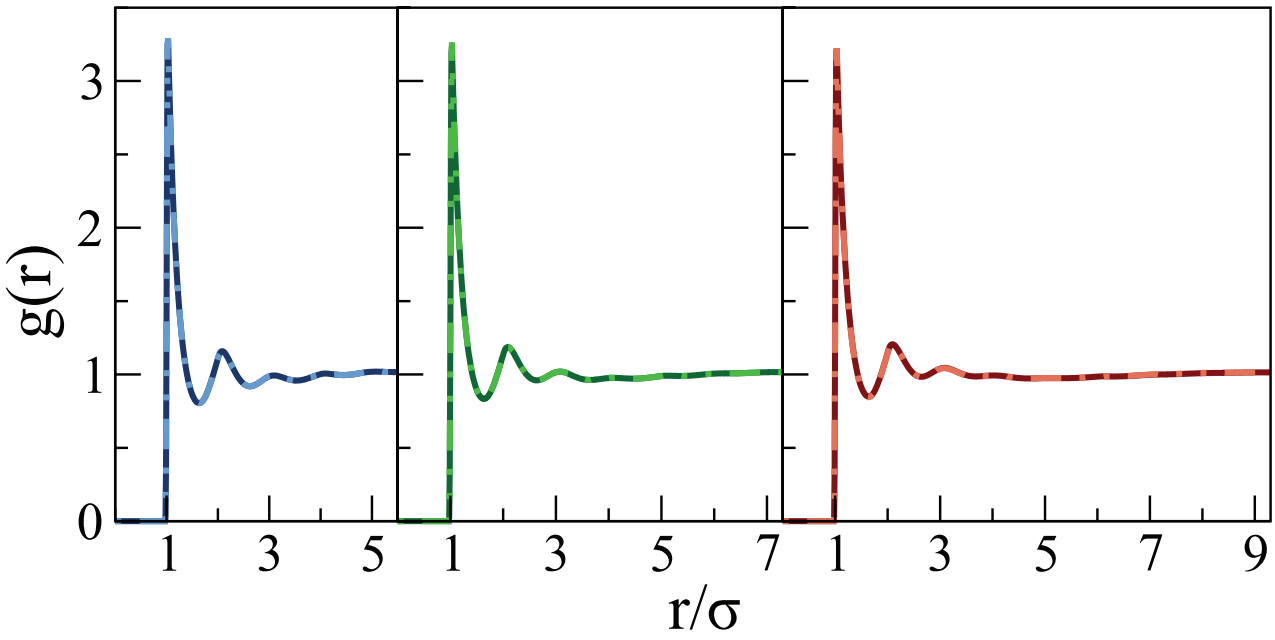

Figure S1: At $\eta_{\text{opt}} = 0.31$, comparison of target (darker) and optimized (lighter) radial distribution functions for $d_{\text{pore}} = 3$ (*left*), 4 (*center*), and 5 (*right*).

Inserted Test Sphere Size Dependence

As described in the main text, we analyze the pores by randomly inserting test spheres that do not overlap with the particles in the simulation. While the choice for the diameter of the test sphere is not unique, there are several considerations. For diameters that are too small, the test spheres will fill in both the pores and the naturally occurring interstitial spaces in the fluid. (This is somewhat analogous to a cluster size distribution for a clustered fluid, where both monomer and very small clusters are in coexistence with larger clusters of a preferred size.) As a result, the volume of the designed pores might be over estimated because the surrounding interstitial spaces might bleed into the the spherical pores. In the limit of infinite test points, all of the void space could be defined as a single pore, regardless of structure. On the other hand, if the test spheres are too large, then effects such as anisotropy and roughness of the pore surfaces might not be captured by the inserted test spheres, making the diameter of the pores artificially smaller.

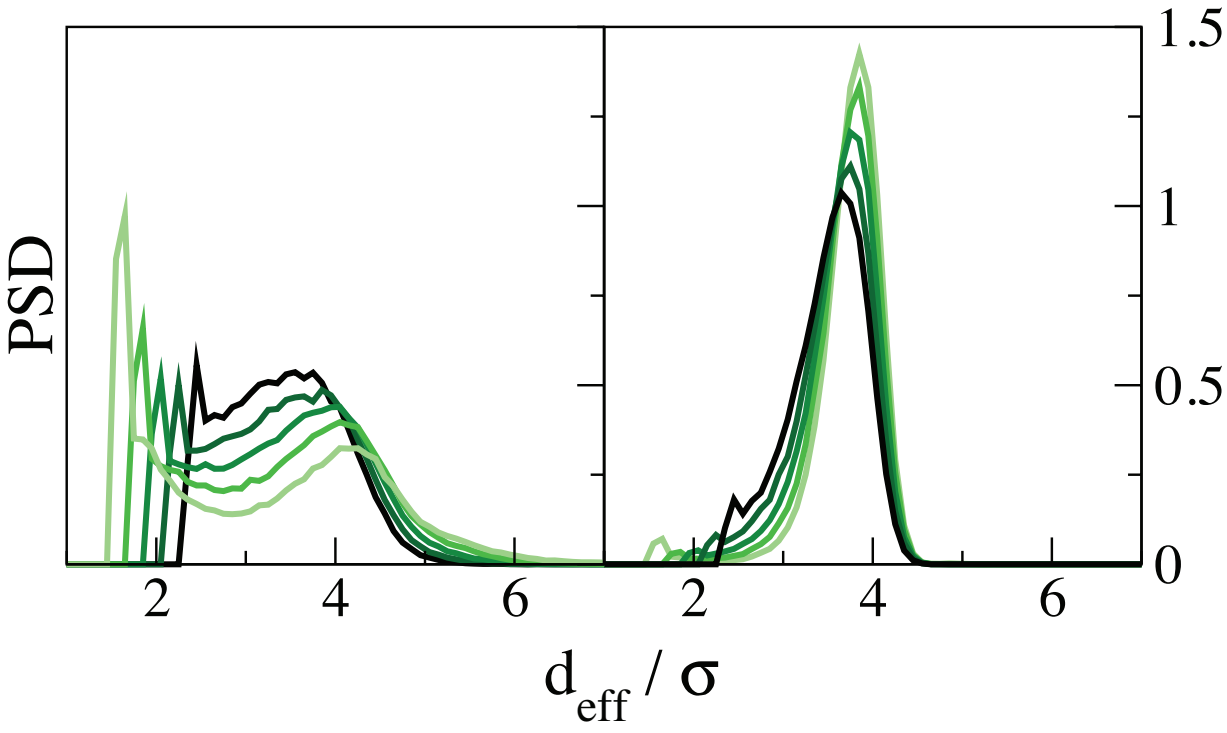

Figure S2: PSD functions for different inserted test sphere diameters (from light to dark: 1.6σ, 1.8σ, 2.0σ, 2.2σ, and 2.4σ) for $d_{\text{pore}} = 4$ and η_{opt} =0.22 (*left*) and 0.31 (*right*).

In Fig. S2, we plot the PSDs for $d_{\text{pore}} = 4$ and $\eta_{\text{opt}} = 0.22$ (left) and 0.31 (right) with a variety of test sphere diameters. As expected, smaller inserted test spheres result in larger pores and vice versa. Throughout, we used test spheres with a diameter of 2σ for the characterization; at approximately this diameter, the artificial peak in the PSD due to the discrete nature of the test spheres is minimized in both cases. As a complementary, though indirect, metric, we note that hard sphere-like simulations (using WCA particles, see Sect. 2.1 in the main text) performed at all η_{opt} values indicated that spherical interstitial spaces of this size were extremely rare (data not shown).

Analysis for $d_{\text{pore}} = 5$ Target

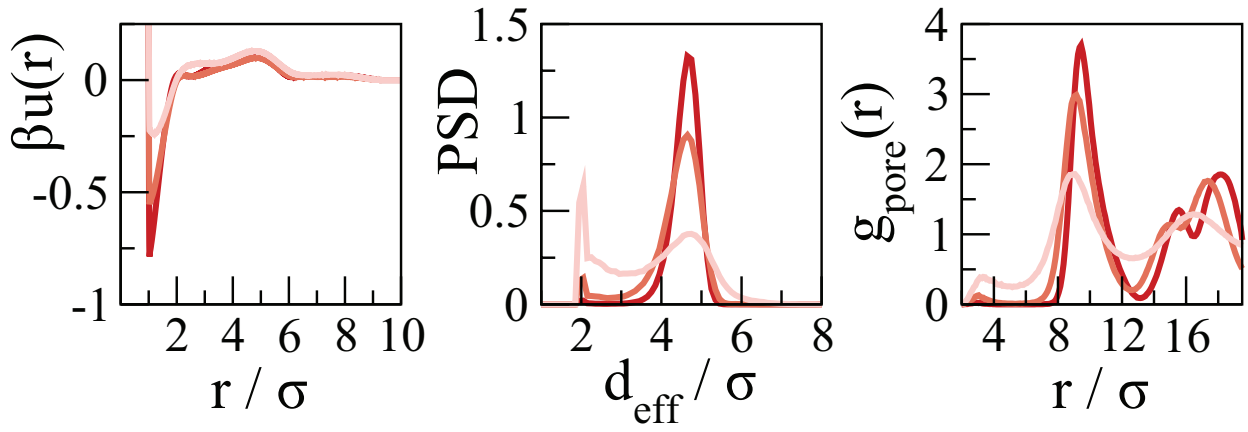

Figure S3: For η=0.22, 0.26, and 0.31 (from light to dark), the dimensionless optimized pair potential, $\beta u(r)$ (*left*), PSD (*center*), and $g(r)$ associated with the pore centers (*right*) for $d_{\text{pore}} = 5$.

As shown in Fig. S3 for η_{opt} =0.22, 0.26, and 0.31, the results for $d_{\text{pore}} = 5$ follow the same trends as η_{opt} increases–increased amplitude of features in the potential, decreased polydispersity of the pores, and onset of pore crystallization–as those presented in the main text.

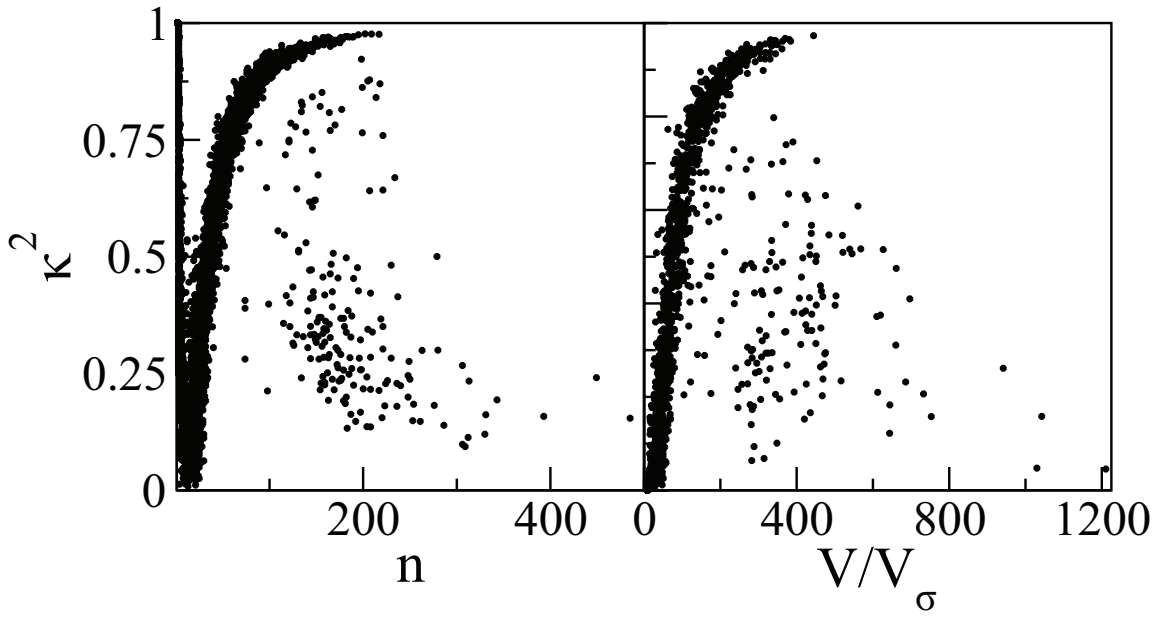

Figure S4: κ^2 as a function of cluster size for the columnar phase shown in Fig. 3b in the main text (*left*) and pore volume (normalized by the volume of a particle with a diameter of σ) for the inverse columnar phase shown in Fig. 3d of the main text (*right*) for 25 simulation snapshots.

Additional Anisotropy Factor Calculations

The κ^2 values shown in Fig. 3f and 4f of the main text are averages for the discrete particle- or void-based objects, weighted by aggregate size and void volume, respectively. Fig. S4 shows κ^2 for the individual particle aggregates (left) and void regions (right) at packing fractions corresponding to particle column and void column phases, respectively. As anticipated in Sect. 2.2 of the main text, it is clear that small particle aggregates have highly variable anisotropy factors, and small voids are effectively spherical because they are typically comprised of only one or a few highly overlapping test sphere(s). Beyond this regime, the anisotropy is more or less directly related to the size of the feature–indicating that the columns (particle aggregate or void) are growing in length. However, for the larger features especially, there is a shift downward in κ^2, likely an artifact of multiple structures being identified as a single feature in the cluster analysis, a consequence of the large interfacial areas between columns. Such large features are heavily weighted in the average, which de-

presses the reported κ^2 values. However, from the data shown in Fig. S4, it is clear that many columns do span the simulation box with the expected κ^2 values near to 1.

The analogous plots to Fig. 3f and 4f for $\eta_{\text{opt}} = 0.22$ and 0.35 are shown in Fig. S5. They follow straightforwardly from $\eta_{\text{opt}} = 0.26$ and 0.31 shown in the main text. For $\eta_{\text{opt}} = 0.22$, the particle-based curve is very similar to Fig. 4f, where the clusters are highly anisotropic (visual inspection reveals that they are amorphous as well). The void spaces are significantly more anisotropic than the $\eta_{\text{opt}} = 0.26$ case, particularly at η_{opt}, indicating even greater discrepancies between the target simulation and the behavior of the optimized potentials as η_{opt} is further reduced. On the other hand, as η_{opt} is increased to 0.35, the microphases are again readily apparent, with columns of both particles and voids indicated by their relatively large κ^2 values at intermediate particle concentrations.

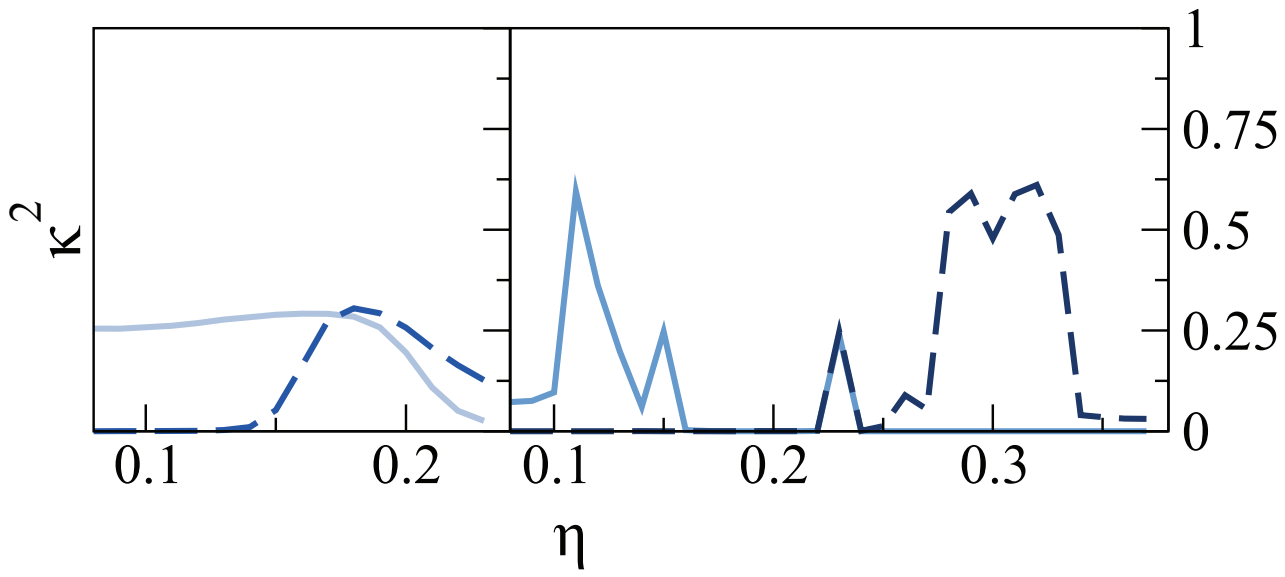

Figure S5: κ^2 as a function of η for potentials optimized at packing fractions of 0.22 (*left*) and 0.35 (*right*).